JOURNAL OF GUIDANCE, CONTROL, AND DYNAMICS
Vol. 30, No. 3, May–June 2007

Dynamics of Circularly Towed Cable Systems, Part 2: Transitional Flight and Deployment Control

Paul Williams* and Pavel Trivailo†
RMIT University, Bundoora, Victoria 3083, Australia

DOI: 10.2514/1.20434

When the towpoint of an aerial cable system moves in a tight circular path, the drogue at the cable tip moves towards the center of the circle, and its altitude decreases relative to its equilibrium position in forward flight. Such a system has both military and civilian applications, including remote pickup and delivery of payloads. This work studies the transitional dynamics of such a system as the aircraft changes from straight flight to circular flight. The system dynamics are modeled using a discretized cable model, allowing the cable to take on zero tension values. Numerical simulation results show that the cable becomes slack during the transition if the aircraft turns too rapidly. Parametric studies of the towpath are performed for both tow-in and tow-out maneuvers. Tension waves can be reduced by appropriate control of the towpoint. Simulated annealing is used to optimize some parameters used to specify the tow-in maneuver. Alternatively, a deployment controller is developed using fuzzy logic that avoids some of these problems by deploying the cable while the aircraft orbits. Instability of deployment for certain combinations of cable length and length rate are observed.

I. Introduction

RAPID access to many remote regions that cannot be reached by helicopters can often be reached easily using aircraft. However, with the exception of vectored thrust aircraft, most aircraft are not versatile enough to allow rescue operations or deployment of supplies to be carried out without landing. Landing an aircraft in remote regions also poses many problems and does not allow for rapid departure from possibly dangerous areas. To overcome some of these difficulties, an aerial-towed cable system has been proposed to allow access to ground regions that are not otherwise accessible [1]. Such a system is composed of a towing vehicle (aircraft), cable, and cable end body (drogue). Towed-cable systems have been studied for well over 50 years and are flown regularly by the U.S. Navy using the E-6A TACAMO. Recent studies point to the possibility of automating the system for payload pickup and delivery [2]. Such a system requires the aircraft to fly tight circular paths around a target location with the tow cable deployed to ground level.

The purpose of this paper is to study the dynamics of a towed circular cable system during the transitional phase between straight, level flight and circular flight. In particular, we seek to compare the performance of the system for achieving the final desired motion of the cable tip by 1) transitioning from straight flight to circular flight with the cable already deployed and 2) deploying the cable from the circling aircraft. At first glance, it may appear that the first option would be the quickest way to achieve the desired motion. However, as will be demonstrated in this paper, for the circle radii and aircraft speeds that give the desired system performance, a straight transition initiates a traveling wave along the cable which causes the cable to become slack near the tip (at the drogue end). In addition, the tip of the cable tends to approach a free-fall condition, which could result in the drogue impacting the ground if the aircraft altitude is not adequately controlled. Hence, it is necessary to look at these options in more detail.

The literature on towed systems includes studies on cable motion for systems towed in straight lines, general three-dimensional motion, and circular motion. Huffman and Genin [3] used a continuum representation of an extensible cable to study the dynamics of a sphere towed from an aircraft at constant speed. The method of characteristics was used to solve the equations of motion and numerical results showed that the transverse motion of the cable was always damped for the range of speeds studied. Phillips [4] shows that transverse waves propagated upwind along the cable are damped, but waves propagated downwind are only slightly damped if the wavespeed exceeds the windspeed. Genin et al. [5] considered the coupling between the transverse motion and longitudinal modes of vibration of a towed cable and showed that the coupling was the result of several interacting effects related to the change in the average tension along the cable, geometric nonlinearities, and centripetal acceleration effects. Equilibrium configurations for the case of a C-141 cargo aircraft towing a modified F-106 fighter were determined by Norris and Andrisani [6]. Their approach was to determine the required tension from the connecting cable for equilibrium of the towed vehicle for a given elevator deflection. The continuous equations representing the cable were then integrated numerically to determine the cable shape. Nakagawa and Obata [7] studied the stability of a towed aerial system using an assumed modes approach with an inextensible cable. Only two-dimensional motion was considered and the towing vehicle was assumed to be flying straight at relatively high speed. Numerical results suggest that a towed sphere can become unstable by way of cable flutter if the size of the sphere is small. Etkin [8] also studied the stability of towed aerial bodies, but considered the effect of cable extensibility. Etkin suggests that bodies that are only subjected to aerodynamic drag are not unstable, but bodies that provide lift and other forces can become unstable. For the example scenario of a pendant vehicle attached at the end of the cable, instability occurs when the cable is attached at the center of gravity (c.g.) of the end body, but the instability may be eliminated by attaching the cable forward and above the c.g. of the towed body. Related interest in the dynamics of tethered aerostats has seen the use of lumped mass models of the tether to study the influence of different turbulence patterns on the motion of the aerostat [9]. The stability of a specific aerostat connected to the ground by a single tether was considered by Lambert and Nahon [10]. The tether was modeled using a lumped mass representation (discretized into 10 elements for the analysis). The stability analysis of the system was conducted by linearizing the dynamic model

Presented as Paper 6125 at the Atmospheric Flight Mechanics, San Francisco, 15–18 August 2005; received 8 October 2005; revision received 4 March 2006; accepted for publication 6 March 2006.

*Research Fellow, School of Aerospace, Mechanical, and Manufacturing Engineering, P.O. Box 71; paul.williams@rmit.edu.au. Member AIAA.

†Professor, School of Aerospace, Mechanical, and Manufacturing Engineering, P.O. Box 71.

around an equilibrium position via a finite difference approximation and analyzing the resulting eigenvalues and eigenvectors for the first four modes of the system. Numerical results for the system frequencies for slow wind speeds showed excellent agreement with analytical results.

Active control of the towed vehicle was considered by Cochran et al. [11] using a variable-length inextensible cable (lumped mass) model. Changes in cable length were accommodated by varying the length of the link closest to the aircraft. Numerical results showed that a passive tow vehicle becomes unstable at the end of retrieval, with a short length of cable on the order of 0.6 m. The instability was stabilized by an autopilot controller on the towed vehicle. The controller was synthesized by linear controllers designed around particular trim conditions, for which a table lookup was used. The tension from the cable, and in particular its variation, was not accounted for explicitly in the control law design. Active control of the towed vehicle has also been considered by Henderson et al. [12]. Bourmistov et al. [13] developed a nonlinear controller for the towed body based on inverting the dynamic and kinematic equations of motion for the towed body by separating the nonlinear system into separate lower order subsystems based on the differences in time scale. More recently, the application of towed systems for low altitude atmospheric research has been considered by Quisenberry and Arena [14]. Control of the towed vehicle for tracking ocean waves was implemented by measuring the height of the ocean waves via a radar altimeter. A proportional-derivative controller, implementing corrections to the wing angle on the tow vehicle, was used to track the ocean waves. The tracking accuracy of the proposed controller depends on the sampling rate of the altimeter. The design of the towed vehicle for this purpose has been considered by Lawhon and Arena [15].

Guidance for an aerial-cable pickup system has been considered by Jun et al. [16]. In their work, a "snatch" pickup was studied, where a towed vehicle with wings and control surfaces was used to guide the cable tip to hook onto a stationary ground target. The extensible cable was modeled with two-dimensional lumped masses. Cable deployment/retrieval was simulated via a tension control mechanism by allowing the last cable segment in the model (attached to the aircraft) to change in length. However, the guidance controller, designed using a linear quadratic digital regulator, was based on knowledge of prescribed cable forces (i.e., the coupling between the cable dynamics and end body control is not incorporated). The control of cable deployment/retrieval for rendezvousing with ground targets has also been examined by Trivailo et al. [17] assuming a straight, rigid cable. Control of the cable deployment for a flexible cable for rendezvous with multiple targets and incorporating collision avoidance has also been developed [18].

Trajectory generation for a circularly towed aerial-cable body system was considered by Murray [19]. Murray has shown that the towed-cable system is differentially flat with the motion of the drogue as the flat output. Thus, the entire motion of the system is characterized by the drogue's motion. In his work, the cable was modeled by rigid links connected to point masses. Numerical results were obtained that showed the required motion of the towplane to achieve commanded motions of the drogue. The effect of a steady wind was also considered, which causes a steady-state offset of the drogue in the horizontal plane and periodic oscillations in the vertical plane. The trajectory of the towplane to eliminate the oscillations was found, but the motion requires nonsmooth (unrealistic) flight characteristics to completely eliminate the effect of the wind. Transitions from one trajectory to another were also considered, but the numerical algorithm suffered from large instabilities for any nondifferentiable motions. A similar scheme for inverting the motion of a towed underwater vehicle was discussed by Hover [20], but the commanded motion was very slow and the drag forces on the system are very much higher than those experienced in an aerial environment. The results were validated in a full-scale towing experiment.

Borst et al. [21] designed a flight controller for the TACAMO mission, which involves an E-6 aircraft flying in a circular orbital pattern with a 5-mile-long trailing wire antenna deployed. The objective of the mission is to maximize the verticality of the cable. The flight controller is designed to compensate for yo-yo oscillations in the towed cable caused by wind shears. A fuzzy logic controller that modifies the aircraft bank angle as a function of aircraft heading is used. The primary feedback parameter is the cable tension at the aircraft end. A lumped mass model of the cable that neglects cable extensibility is used to simulate the controller. Numerical results illustrate excellent control of the system. Brushwood et al. [22] discuss the implementation of the "orbit improvement system," which has been implemented fleetwide since 1997.

Deployment control of an aerial-cable munition system was considered by Frost and Costello [23] using a lumped mass model of the cable. The cable deployment is governed as a function of reel resistance forces, which are defined either as functions of the amount of cable deployed or the deployment rate. Parameters in the resistance forces are optimized to reduce loads in the cable, the acceleration of the follower projectile and the time taken for the system to reach a steady state.

The rich literature base on aerial-cable systems is also supported by repeated successful flight demonstrations, such as the E-6A orbit improvement missions. An early application of aerial-cable systems for picking up payloads was developed by Lytle Adams and Boeing engineers in 1928. The idea used a Stinson aircraft with a deployed boom to pick up a cargo container that was attached to a rope connected between two poles (14 ft high and 20 ft wide). A hook at the end of the boom engaged the rope and additional rope was deployed from a winch to absorb the shock. The rope and payload were subsequently reeled back into the aircraft. This method was used to deliver express mail in the United States during the 1930–1950 period by All American Aviation [24]. One disadvantage of this method is that the hook used to engage the rope was located to the rear of the pilot. An alternative method that was employed to extract crew from remote locations was the "Fulton Skyhook." This method used a "skyanchor" on the nose boom of the aircraft to hook onto a line hoisted by a helium balloon. The payload was attached at the end of the line [25].

The original idea of deploying a cable from a circling aircraft to achieve stationary or near-stationary motion of the endpoint was invented by Nate Saint. Nate Saint was a pilot in the mid-1950s with the Missionary Aviation Fellowship whose job involved delivering gifts, food, and clothing to a tribe of Indians in Ecuador. Rather than dropping the items from the aircraft, a canvas bag with the items was lowered from the circling aircraft to a near-stationary point on the ground, where the items were retrieved [26]. A more detailed review of the literature on this concept may be found in Part 1 [27]. This type of towed aerial system provides a possible means for achieving a wide range of important applications, such as 1) airborne search and rescue operations, 2) precision airborne delivery of supplies to remote locations, 3) water bombing of bushfires, and more [1]. An approach for designing the system given aircraft performance constraints is dealt with in Part 1 [27]. The work of Williams and Trivailo [27] focused primarily on the equilibrium and stability of optimal, practical configurations. There has been relatively little focus on the dynamics of such a system during the transition phase from straight flight to circular flight, and vice versa, and for deployment of the cable. This is the focus of this paper.

II. Mathematical Model of Towed-Cable System

Cable-body systems have been studied in virtually all operating conditions: air, sea, and space. Each environment has specific dynamical features that must be carefully accounted for. Two modeling approaches have been used to model the complex cable dynamics: continuum models [28–32] and lumped mass models [33–39]. The approaches have been compared [40] and although it is believed that the continuum model provides the most accurate representation of the cable, the lumped mass model is the most versatile and simplest to program. The equilibrium and stability of a circularly towed system was studied using a lumped mass model in [27]. Because the model in [27] focused purely on the circular portion of the flight rather than arbitrary flight conditions and used a rotating

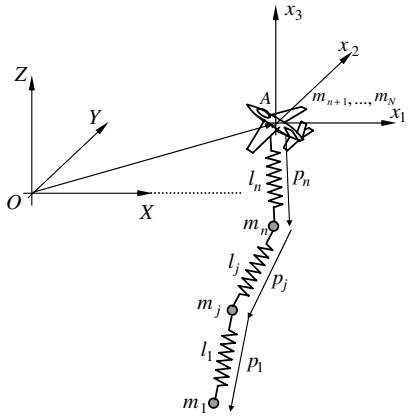

Fig. 1 Lumped mass cable representation and element numbering.

coordinate system, it is more convenient to use an alternative mathematical model in this Part. Furthermore, in Part 1, damping forces were neglected for the stability analysis, and the cable tension forces were assumed to be always positive. Because the dynamics of the cable for transitional maneuvers involve large changes in geometry of the cable, it is necessary to consider situations that involve slack cables. In addition, internal damping in the cable is introduced to damp the cable longitudinal vibrations. In general, faster propagation of equations is possible by including some damping in the system, with minimal impact on the overall motion of the system (see Sec. IV).

The physical system, which consists of a host aircraft, cable and drogue may be represented mathematically as shown in Fig. 1. The inertial coordinate system with origin O is denoted by (X, Y, Z), and the cable dynamics are expressed in a translating, nonrotating coordinate system $(\boldsymbol{x}_1, \boldsymbol{x}_2, \boldsymbol{x}_3)$ with origin at A which is aligned with the inertial coordinate system. As such, the unit vectors $\boldsymbol{x}_1, \boldsymbol{x}_2$, and $\boldsymbol{x}_3$ may be considered inertial reference directions. The point masses, which represent the cable, are numbered from 1 at the drogue through to n, representing the last cable element deployed from the aircraft, as shown in Fig. 1. It is assumed that the remaining undeployed cable remains with the aircraft, and hence elements $n+1, \ldots, N$ translate with the aircraft, where N is the maximum number of discrete cable elements. The masses are connected via viscoelastic springs that model the cable elasticity and internal damping forces. Note that the model does not incorporate active aircraft dynamics; rather, the purpose of the study is to examine the effects of the towpoint motion itself on the cable dynamics.

A. Kinematic Equations

The generalized coordinates for the system lumped masses are chosen as the scalar components of the relative displacement of mass j from mass $j+1$. This displacement vector, shown in Fig. 1, can be written as

$$\boldsymbol{p}_j = q_{3(j-1)+1}\boldsymbol{x}_1 + q_{3(j-1)+2}\boldsymbol{x}_2 + q_{3(j-1)+3}\boldsymbol{x}_3, \qquad j = 1, \ldots, n \tag{1}$$

where $q_{3(j-1)+i}, (i = 1, 2, 3; j = 1, \ldots, n)$ are the generalized coordinates. The generalized speeds are chosen as the inertial velocities of each lumped mass. This selection of generalized coordinates and generalized speeds gives the kinematic equations

$$\dot{q}_{3(j-1)+i} = u_{3(j-1)+i} - u_{3+i} \qquad i = 1, 2, 3; \quad j = 1, \ldots, n-1 \tag{2a}$$

$$\dot{q}_{3(n-1)+i} = u_{3(n-1)+i} - \dot{x}_i \qquad i = 1, 2, 3; \quad j = n \tag{2b}$$

where $u_{3(j-1)+i}, (i = 1, 2, 3; j = 1, \ldots, n)$ are the generalized speeds and $\dot{x}_i (i = 1, 2, 3)$ are the velocity components of the host aircraft. Note that in the model the motion of the aircraft is specified by the Cartesian components of the aircraft velocity $\dot{x}_i, i = 1, 2, 3$. This simplifies the analysis because it is typically easier to specify velocities than to specify accelerations. However, with such an approach it is necessary to provide continuous velocity profiles for the aircraft to ensure realistic results.

B. Force Equations

By a straightforward application of Newton's second law, the time derivatives of the generalized speeds are easily obtained in terms of the components of the external forces. The force equations are given simply by

$$\dot{u}_{3(j-1)+1} = \frac{1}{m_j}\left[F^s_{3(j-1)+1} + F^d_{3(j-1)+1} + F^{\text{aero}}_{3(j-1)+1}\right] \tag{3}$$

$$\dot{u}_{3(j-1)+2} = \frac{1}{m_j}\left[F^s_{3(j-1)+2} + F^d_{3(j-1)+2} + F^{\text{aero}}_{3(j-1)+2}\right] \tag{4}$$

$$\dot{u}_{3(j-1)+3} = \frac{1}{m_j}\left[F^s_{3(j-1)+3} + F^d_{3(j-1)+3} + F^{\text{aero}}_{3(j-1)+3} + F^g_{3(j-1)+3}\right] \tag{5}$$

where m_j is the elemental mass of the jth cable segment, defined by

$$m_j = \begin{cases} m_d + \rho A L_{s_1}/2, & j = 1 \\ \rho A (L_{s_j} + L_{s_{j-1}})/2, & j = 2, \ldots, n \end{cases} \tag{6}$$

where ρ is the density of the cable material, A is the cable cross-sectional area, and L_{s_j} is the unstrained length of the jth cable segment. The generalized forces on the right-hand side of Eqs. (3–5) are due to tension/spring forces, damping forces, aerodynamic drag forces, and gravity forces, denoted by the superscripts s, d, aero, and g, respectively. The gravitational and aerodynamic forces are defined in Part 1 [27] and are not repeated here for the sake of brevity.

1. Tension Forces

There are certain circumstances where the cable may lose tension. However, because a cable cannot sustain compression forces (by assumption) it is necessary to prevent such forces from occurring in the dynamic model. Thus, the strain in the jth segment is defined by

$$\varepsilon_j = \begin{cases} \frac{|\boldsymbol{p}_j| - L_{s_j}}{L_{s_j}}, & |\boldsymbol{p}_j| \geq L_{s_j} \\ 0, & |\boldsymbol{p}_j| < L_{s_j} \end{cases} \tag{7}$$

Extensive numerical simulations reveal that this scheme alone slows the numerical integration considerably and can cause failure of some integration routines. To overcome this we define the tension in the jth segment according to the following modified scheme in conjunction with Eq. (7):

$$T_j = \begin{cases} \text{EA}\left(3\varepsilon_j^5/\varepsilon^{*4} - 8\varepsilon_j^4/\varepsilon^{*3} + 6\varepsilon_j^3/\varepsilon^{*2}\right), & 0 \leq \varepsilon_j \leq \varepsilon^* \\ \text{EA}\varepsilon_j, & \text{otherwise} \end{cases} \tag{8}$$

Equation (8) modifies the tension in cases where the strain approaches zero. The strain ε^* is the lower bound on the strain where Hooke's law applies. Below this value, the tension is modified so that the slope of the stress-strain curve has continuous first- and second-order derivatives at the boundary points $\varepsilon = (0, \varepsilon^*)$, as well as matching the tension values at these points. This ensures that the tension-strain curve for each cable element has continuous derivatives to second order.

The total force due to tension on the jth mass is given by

$$\boldsymbol{F}^s_j = T_{j-1}\frac{\boldsymbol{p}_{j-1}}{|\boldsymbol{p}_{j-1}|} - T_j\frac{\boldsymbol{p}_j}{|\boldsymbol{p}_j|} \tag{9}$$

and $F^s_{3(j-1)+i} \triangleq \boldsymbol{F}^s_j \cdot \boldsymbol{x}_i, i = 1, 2, 3$.

2. Damping Forces

The damping forces in the cable are assumed to be proportional to the strain rate. The length of the jth segment may be expressed as

$$l_j = L_{s_j}(1 + \varepsilon_j) \tag{10}$$

The time derivative of Eq. (10) is given by

$$\dot{l}_j = \dot{L}_{s_j}(1 + \varepsilon_j) + \dot{\varepsilon}_j L_{s_j} \tag{11}$$

Upon rearranging this we obtain

$$\dot{\varepsilon}_j = \frac{\dot{l}_j}{L_{s_j}} - \frac{\dot{L}_{s_j}}{L_{s_j}}(1 + \varepsilon_j) \tag{12}$$

The derivative of the length of the jth segment is obtained by projecting the derivative of the relative vector between mass j and mass $j + 1$ along the direction of j,

$$\dot{l}_j = \dot{\boldsymbol{p}}_j \cdot \frac{\boldsymbol{p}_j}{|\boldsymbol{p}_j|} \tag{13}$$

By using the relation $|\boldsymbol{p}_j| = L_{s_j}(1 + \varepsilon_j)$, Eq. (12) can be expressed as

$$\dot{\varepsilon}_j = \frac{\sum_{i=1}^{3} q_{3(j-1)+i}\dot{q}_{3(j-1)+i}}{L_{s_j}\sqrt{\sum_{i=1}^{3} q_{3(j-1)+i}^2}} - \frac{\dot{L}_{s_j}\sqrt{\sum_{i=1}^{3} q_{3(j-1)+i}^2}}{L_{s_j}^2} \tag{14}$$

The damping force in the jth segment is given by

$$D_j = \begin{cases} C\dot{\varepsilon}_j, & \varepsilon_j \geq 0 \\ 0, & \varepsilon_j < 0 \end{cases} \tag{15}$$

where C is the cable damping coefficient. The total force due to damping on the jth mass is

$$\boldsymbol{F}_j^d = D_{j-1}\frac{\boldsymbol{p}_{j-1}}{|\boldsymbol{p}_{j-1}|} - D_j\frac{\boldsymbol{p}_j}{|\boldsymbol{p}_j|} \tag{16}$$

and $F_{3(j-1)+i}^d \triangleq \boldsymbol{F}_j^d \cdot \boldsymbol{x}_i$, $i = 1, 2, 3$.

C. Deployment/Retrieval Modeling

The cable is modeled using discrete elements, so incorporating deployment and retrieval is a matter of adding and subtracting elements from the model. Essentially, the length of the nth cable segment L_{s_n} is adjusted according to a length control law. When the length of the nth segment is greater than some upper bound, a new cable element is introduced with initial conditions such that the tension across the nth and $(n + 1)$th segments is maintained. The velocity of the new mass is determined so as to maintain constant velocity along the cable tangent direction, and the velocity components normal to the cable are modified so as to maintain constant angular velocity of the new segment(s). For retrieval, when the nth segment reduces below a given threshold, the nth mass is removed and the length of the $(n - 1)$th segment is updated. This approach works very well for tethered satellite systems, where the dominant forces are from the gravity-gradient, Coriolis forces, and tension. However, for an aerial-cable system, some small bouncing of the new mass occurs because of the dominance of aerodynamic drag.

III. Transitional Flight and Cable Deployment Control

A. Transitional Flight

A typical maneuver consists of the following stages: 1) straight, level flight towards the target region; 2) transitional flight around the target ("tow-in"); 3) stationkeeping (circular) flight around the target; 4) transitional flight to enlarge the circle ("tow-out"); and 5) return to straight, level flight. For a given aircraft and cable configuration, the stationkeeping phase is essentially fixed by the optimal system parameters, as discussed in Part 1 (see [27]).

To study the transition from straight to circular flight, a relatively simple variation in the towpoint velocity is considered. The model described in Sec. II allows any motion of the towpoint to be specified, but for the purposes of this initial study the towpoint motion is assumed to occur at constant altitude. To ensure that the towpoint motion can be flown by a real aircraft, the velocity is assumed to be constant throughout the maneuver. For general two-dimensional flight around the origin, we have the following kinematic equations for the aircraft in terms of polar coordinates,

$$x_1 = R\cos\theta, \qquad x_2 = R\sin\theta \tag{17}$$

$$\dot{x}_1 = \dot{R}\cos\theta - R\dot{\theta}\sin\theta, \qquad \dot{x}_2 = \dot{R}\sin\theta + R\dot{\theta}\cos\theta \tag{18}$$

where R is the instantaneous radius of the orbit and θ describes the angular rotation of the aircraft around the orbit. Note that Eq. (18) can be used for general two-dimensional motion around an arbitrary fixed point. Thus, a typical tow-in maneuver would be specified as follows:

$$\dot{x}_1 = \begin{cases} V & \text{straight flight} \\ \dot{R}\cos\theta - R\dot{\theta}\sin\theta & \text{tow-in} \\ -R\dot{\theta}\sin\theta & \text{circular flight} \end{cases}$$

$$\dot{x}_2 = \begin{cases} 0 & \text{straight flight} \\ \dot{R}\sin\theta + R\dot{\theta}\cos\theta & \text{tow-in} \\ R\dot{\theta}\cos\theta & \text{circular flight} \end{cases} \tag{19}$$

The potential importance of ensuring a well-selected transition from forward flight to circular flight was observed during initial simulations of a towed system with arbitrarily selected parameters: cable discretization 20 elements, cable length 3 km, drogue mass 10 kg, cable diameter 2 mm, cable mass density 3000 kg/m^3, aircraft speed 25 m/s, circle radius 300 m, damping coefficient 500 Ns, and cable slack parameter $\varepsilon^* = 10^{-6}$. As shown in Figs. 2–4, without proper control the cable can become slack when the aircraft turns too quickly. The trailing cable has a tendency to "come back" onto itself. This situation creates local regions where the cable relative velocity drops sharply, causing a sudden drop in tension due to the rapid change in drag forces. A traveling wave is initiated that travels along the cable down to the drogue, which is essentially in a free-fall condition due to the absence of tension forces.

Figure 2 shows the cable tension at the drogue and aircraft ends of the cable during the maneuver. It is evident that there is a significant

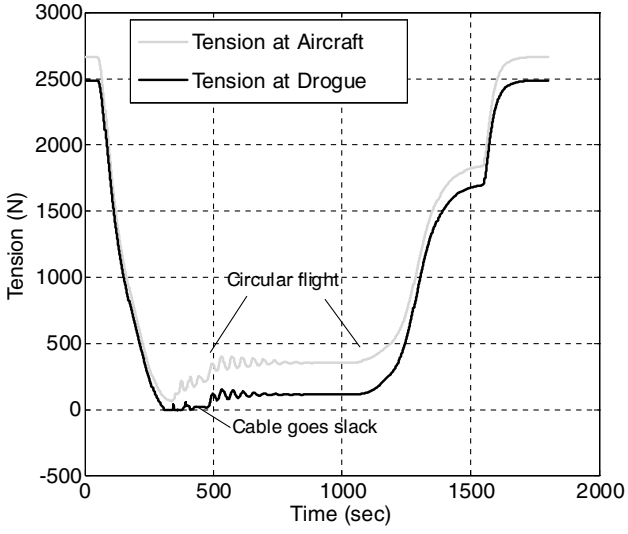

Fig. 2 Cable tension during transition into and out of circular flight.

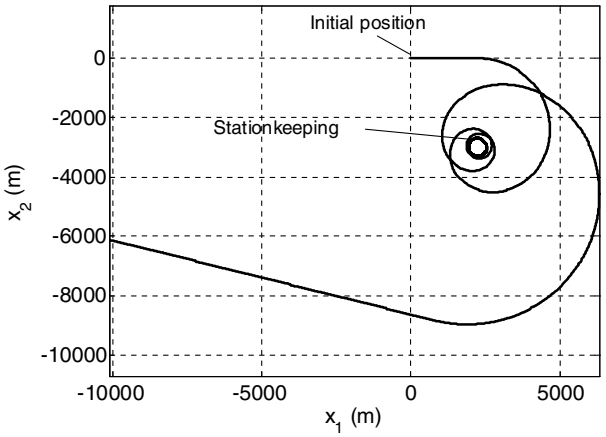

Fig. 3 Flight path for transition into and out of circular flight.

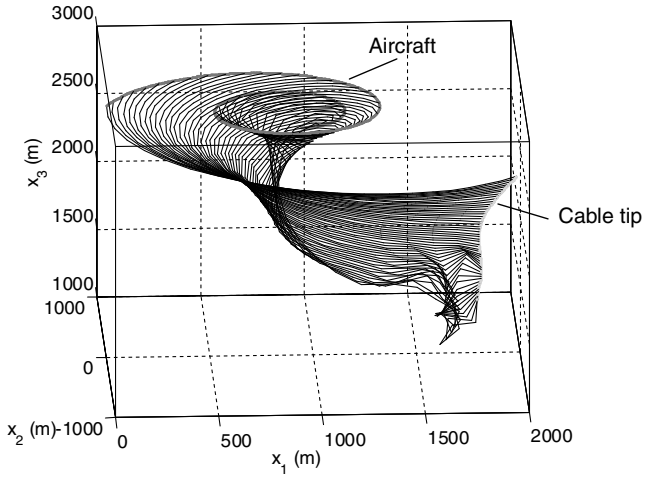

Fig. 4 Cable shape during initial phases of transition into circular flight.

gradient in tension along the cable due to cable weight and aerodynamic drag, which is most significant during circular flight due to the large differences in velocity of the cable near the aircraft and drogue. The aircraft flies straight initially, then after 50 s it initiates the tow-in maneuver. This causes a dramatic drop in tension, ultimately causing the cable to become slack at the drogue end. Figure 3 shows the flight path of the aircraft, and Fig. 4 shows the cable shape during a portion of the transition. Initially, the cable maintains a good, curvilinear shape. However, when the aircraft turns back rapidly, the cable is still in the midst of adjusting to the initial change in heading. The significant curvature of the cable creates a condition where the cable takes on multiple turns. Figure 4 shows the effect of a slack cable at the drogue, with significant distortions to the cable shape. Because the aircraft enters into circular flight well before the drogue, the drogue undergoes a series of oscillations in the vertical plane. The drogue gradually "sinks" to the desired altitude. The major cause of this phenomenon is due to the changes in aircraft heading. When the aircraft is flying back towards the drogue position, there tends to be a drop in tension (i.e., the distance between the aircraft and drogue decreases). When the aircraft is flying away from the drogue position, the tension increases (i.e., the distance between the aircraft and drogue increases). These oscillations are visible in the tension variation in Fig. 2. It is these dynamical effects that motivated a more detailed study of the transitional dynamics. It should also be noted that this behavior has been observed by the authors during flight tests with a model aircraft.

If the aircraft transitions quickly from straight flight to circular flight at the desired radius with the cable deployed, then a traveling wave is initiated that causes the cable to become slack. Hence, it may be preferable to perform the maneuver more slowly by transitioning from straight flight to circular flight at a radius much larger than the desired radius. The aircraft can then be progressively flown in tighter circles by slowly spiraling inwards. This can be achieved by scheduling R slowly, either linearly or with a cosine-type variation. The total aircraft velocity is constant in these scenarios and is given by

$$V^2 = \dot{R}^2 + R^2\dot{\theta}^2 \Rightarrow \dot{\theta} = \sqrt{\frac{V^2 - \dot{R}^2}{R^2}} \tag{20}$$

Differentiating Eq. (20) gives

$$\ddot{\theta} = -\left(\frac{\dot{R}\,\ddot{R}\,R^2 + R\dot{R}(V^2 - \dot{R}^2)}{R^4\dot{\theta}}\right) \tag{21}$$

In this paper, two variations in the orbit radius are considered. The first is a simple cosine-type variation given by

$$\begin{aligned} R &= \frac{(R_0 - R_f)}{2}\cos[\pi(t - t_1)/\Delta t] + \frac{R_0 + R_f}{2} \\ \dot{R} &= -\frac{\pi(R_0 - R_f)}{2\Delta t}\sin[\pi(t - t_1)/\Delta t] \end{aligned} \tag{22}$$

where R_0 is the radius at the beginning of the transition at time t_1, R_f is the final value of the orbit radius, and Δt is the total time for the transition. Equations (22) are used to perform a simple parametric study of the transition. The goal of the study is to determine the influence that the transitional flight path has on the cable dynamics. Hence the free parameters in Eq. (22) are varied in the context of the typical maneuver outlined at the beginning of this subsection. The second variation in orbit radius is optimized to produce a combination of short transition time and minimum traveling waves, as described in the following subsection.

B. Optimal Transitional Maneuvers

The parameters used in Eq. (22) for scheduling the orbit radius during tow-in could potentially be used as optimization parameters. However, in Eq. (22) there are only two parameters that can be varied (R_0 and Δt) because t_1 does not play any role in the tow-in dynamics. To provide more flexibility, a polynomial profile with endpoint constraints is used here. To ensure that the function is well behaved, we employ Chebyshev polynomials as the basis functions and expand the orbit radius function as

$$R := \frac{a_0}{2} + a_1 T_1^c[\tau(t)] + a_2 T_2^c[\tau(t)] + \ldots + a_n T_n^c[\tau(t)] \tag{23}$$

where T_j^c is the jth degree Chebyshev polynomial, which satisfies the recurrence relation

$$\begin{gathered} T_0^c(\tau) = 1, \qquad T_1^c(\tau) = \tau \qquad T_j^c(\tau) = 2\tau T_{j-1}^c(\tau) - T_{j-2}^c(\tau) \\ j > 1 \end{gathered} \tag{24}$$

Note that Chebyshev polynomials are defined on the domain $\tau \in [-1, 1]$, and the orbit radius is an implicit function time through the domain transformation

$$t = \left(\frac{t_2 - t_1}{2}\right)\tau + \left(\frac{t_2 + t_1}{2}\right) \tag{25}$$

In Eq. (23), we must map $\tau(t)$ according to the inverse transformation of Eq. (25).

The a_n polynomial coefficients are determined by several constraints. For example, it is desired to have

$$\begin{gathered} R(t_1) = R_0, \qquad \dot{R}(t_1) = 0, \qquad \ddot{R}(t_1) = 0 \qquad R(t_2) = R_f \\ \dot{R}(t_2) = 0, \qquad \ddot{R}(t_2) = 0 \end{gathered} \tag{26}$$

In addition to these constraints, three interior points are used to help shape the orbit radius. The points are selected based on optimal

interpolation characteristics as $\tau = [-\sqrt{3/7}, 0, \sqrt{3/7}]$. Thus, there are nine pieces of information and $n \geq 9$. Additionally, we desire that the function be "smooth," so n is selected to be 12 and the additional equations are generated by minimizing the cost

$$J = \int_{-1}^{1} \ddot{R}^2 \, \mathrm{d}\tau \tag{27}$$

The endpoint constraints and interior point constraints are appended to Eq. (27) by means of Lagrange multipliers. The resulting set of necessary conditions are generated by taking partial derivatives of the augmented cost with respect to the unknown coefficients and Lagrange multipliers. The resulting set of necessary conditions are linear in the unknown coefficients and multipliers and can be solved easily. In this way, the transition problem becomes one of optimizing the parameters $z = [t_2, R_0, R(\tau = -\sqrt{3/7}), R(\tau = 0), R(\tau = \sqrt{3/7})]$ to minimize some selected performance index.

As demonstrated in Sec. III.A, the variation in tension gives a very good indication of the cable transition dynamics. That is, in straight flight, the cable tension is relatively large due to the significant drag acting on the cable. However, in circular flight, the cable tip is nearly motionless and the drag is considerably reduced from straight flight. Hence, for a smooth transition the cable tension should vary quickly and smoothly from the tension in level flight to the tension in circular flight, while remaining above zero. Based on this, a good performance measure for optimizing the transition dynamics is to minimize the undershoot of the cable tension as well as the transition time. Hence, the cost (to be minimized) is selected as

$$J_1 = -\frac{1}{t_2} \min T \tag{28}$$

which combines both objectives into one nonlinear expression. Because of the high degree of complexity of the system and the nonsmooth cost, the optimization is performed using simulated annealing (SA). SA is a stochastic optimization technique that relies only on function evaluations. The initial solution vector is typically selected randomly. During the solution process, a random displacement is applied to the solution vector. If the new solution vector gives a lower cost than the previous one, it is accepted unconditionally. If the cost of the new potential solution is greater, however, the new solution is accepted probabilistically. The probability of acceptance is determined as a function of the annealing temperature. An annealing schedule is given that dictates the decrement of temperature over time. The higher the temperature the more likely the solution vector is to accept an increase in cost. In this way, the algorithm is able to escape from local minima and move towards the global minimum. Reduction of the temperature logarithmically guarantees an optimal solution. As the temperature reduces to zero, only solutions that lead to a decrease in cost are accepted. It is often necessary, particularly when the number of decision variables is large, to perform the optimization several times to assure global convergence. In the following results, the annealing temperature was selected as 10,000 K, and the reduction in temperature during each iteration was selected as 95%.

C. Cable Deployment Control

In past studies on the subject, relatively little focus has been on controlling the deployment/retrieval processes of the cable. One exception is [41], where a fuzzy logic control algorithm was developed to control the cable winch rate. The main problem with controlling the cable winch rate directly is that it can lead to very high accelerations at the reel that would be unlikely to be achieved in practice. This may be undesirable in critical situations, possibly causing overshoot in the drogue altitude. A better approach is to control the cable winch acceleration under given limits, which might be more meaningful when translating the controller to a winch actuated via torque motors.

The objective of the controller is to deploy the cable at a safe rate so that the drogue enters into a stable orbit close to the ground target. The controller can then hold the cable in relative equilibrium by ceasing deployment/retrieval. It is then desirable to retrieve the cable and drogue at a future time. Several different approaches for controlling the deployment/retrieval of the cable were implemented. It is possible to control deployment using a proportional-derivative type controller. A controller can be designed to minimize the error in the cable tip position by deploying the cable when the tip of the cable is pointing in the desired direction. The major problem with this implementation is that it requires knowledge of the cable shape at the drogue and that it is not robust to the drogue altitude. From a practical point of view, it is much more important to control the altitude of the drogue through cable deployment/retrieval. Furthermore, the altitude is the critical parameter to control for avoiding the drogue from hitting the ground with significant force. For these reasons, the controller developed in this section is based on feedback of the drogue altitude error and altitude (or length) error rate.

1. *Heuristic Control Law*

The first strategy we will consider is a heuristic control law, based on the idea that the winch controller should deploy the cable at the maximum rate for the majority of the deployment, then slow the deployment as the cable tip approaches the desired altitude. The cable tip should then approach the desired altitude asymptotically, similar to the flare maneuver of a landing aircraft. Although a number of different controllers were tested, the following gave reasonably good results:

$$\ddot{L} = \begin{cases} k_1[\dot{L}_c(\Delta h) - \dot{L}], & \Delta h \geq \Delta h_c \\ k_1[\dot{L}_c(\Delta h) - \dot{L}] + k_2 \Delta h, & \Delta h < \Delta h_c \end{cases} \tag{29}$$

where k_1 and k_2 are control gains, $\Delta h = h_{\text{end}} - h_d$, h_{end} is the altitude of the cable tip, h_d is the desired altitude of the cable tip, Δh_c is a critical altitude where the cable tip is close to the target, and $\dot{L}_c$ is the commanded length rate which is scheduled as a function of the altitude error according to

$$\dot{L}_c = \begin{cases} \dot{L}_{\max}, & \Delta h \geq \Delta h_t \\ -\dot{L}_{\max}, & \Delta h \leq -\Delta h_t \\ -\frac{\dot{L}_{\max}}{2} \cos[\pi(\Delta h + \Delta h_t)/\Delta h_t] - \frac{\dot{L}_{\max}}{2}, & -\Delta h_t < \Delta h \leq 0 \\ \frac{\dot{L}_{\max}}{2} \cos[\pi(\Delta h + \Delta h_t)/\Delta h_t] + \frac{\dot{L}_{\max}}{2}, & 0 < \Delta h < \Delta h_t \end{cases} \tag{30}$$

The variation in the commanded length rate inside the "transition" altitude envelope Δh_t, which is the range of altitudes where the deployment rate changes from its maximum value to a smooth variation to avoid excessive overshoot and changes in reel acceleration, is shown in Fig. 5.

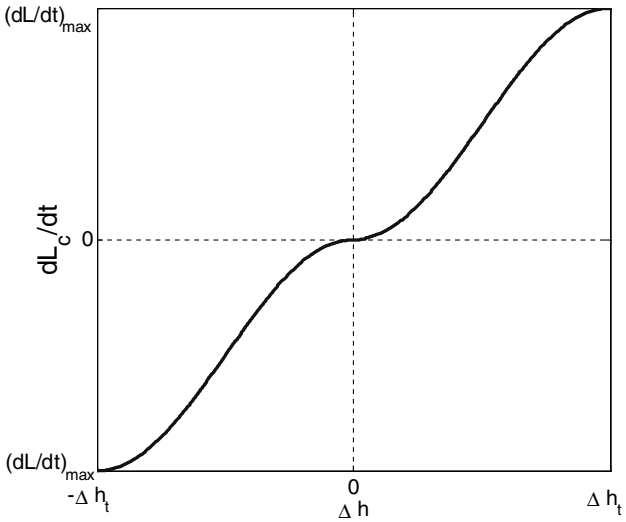

Fig. 5 Variation in commanded length rate inside the transition altitude envelope.

The cable is an elastic body, so there is likely to be some overshoot in the altitude of the cable tip in some situations. Therefore, when deploying the cable in a circular orbit, a two-stage process is used. First, a sufficiently low altitude is commanded (h_0) with ample tolerance to allow some overshoot of the altitude of the cable tip. The deployment is carried out until the tip is reasonably well stabilized at this altitude, typically to within a few meters. The cable tip is then commanded to follow a linear variation in altitude from h_0 to h_f, which is the final desired altitude of the tip. It has been found that this process leads to very small final oscillations of the cable tip in the vertical plane and helps to prevent the drogue from impacting the ground. Although conceptually this process alone should be sufficient, numerical simulations show that for the system configuration being considered here, the cable develops some lateral instabilities during the final stages of deployment. The cause of this is discussed in the Numerical Results section, but it was found necessary to slow the deployment when the cable has been deployed beyond a certain critical length L_{crit}. Hence, $\dot{L}_{\max}$ is not constant in the control law and has a switch to a reduced value, which is a function of the deployed cable length.

2. Fuzzy Logic Control Law

Intelligent controllers, often called soft controllers, can be used to control a broad range of dynamical systems, including those that do not have well-defined system models [42]. Fuzzy logic is a control architecture based on fuzzy conditional rules that is easy to understand and can produce controllers that can be easier to tune and adapt than conventional proportional-derivative (PD) controllers. A winch rate control law was developed in [41] for deployment/retrieval of the cable using fuzzy logic. No instabilities were observed in the model used in [41] using the proposed winch controller. The main reason is due to the slowing of the deployment rate as the desired altitude is approached. Furthermore, very little overshoot was observed in the altitude profile, so the controller is reconsidered here. It is likely that similar performance could be achieved using conventional PD controllers, but the fuzzy logic approach was found to produce the desired results with little expert tuning and will be used in this section.

As mentioned, it is much more desirable to use the winch acceleration, rather than the length rate itself. Hence, the control law is given according to a simplified version of Eq. (29),

$$\ddot{L} = k_1[\dot{L}_c^{\text{fuzzy}}(\Delta h, \Delta\dot{h}) - \dot{L}] \tag{31}$$

where the commanded length $\dot{L}_c^{\text{fuzzy}}$ is scheduled via a fuzzy logic rule-base and is described in the following paragraphs.

Fuzzy controllers, which have been used widely in the control of consumer products, are based on the principles of fuzzy logic introduced by Zadeh [43]. Fuzzy controllers are based on qualitative descriptions of the system to generate sets of rules and consequences, usually in the form of if-then statements. The primary purpose of the fuzzy controller is to map the input space to an output space, so that the output behaves in some desired manner. Fuzzy controllers tend to have structures of the form: preprocessing, fuzzification, rule-base and inference engine, defuzzification, and postprocessing. Each stage within this structure can have different components depending on the complexity of the system. In this section, only the relevant details concerning the control implementation for the towed-cable system is presented.

Preprocessor: In the preprocessor, the key information regarding the system is synthesized. In this work, the preprocessor consists of setting the desired altitude for the drogue, and scaling the error in the drogue's altitude and velocity by the altitude of the aircraft. This makes the controller capable of operation for virtually any cable length.

Fuzzification: The input data, in this case the normalized drogue altitude error and altitude error rate, are fuzzified via input membership functions that determine the degree of membership within the input fuzzy sets. For example, the drogue altitude error membership functions are shown in Fig. 6, where *N*, SN, SP, and *P* are abbreviations of negative, small negative, small positive, and positive, respectively. The rule-base is a set of conditions and consequences that are used to regulate the control signal. In this paper, the rules are defined in Table 1. Table 1 may be interpreted to mean, for example, if the altitude error is positive (*P*) and the change in altitude error is zero, then the deployment rate should be positive (*P*). During the inference step, the inference engine determines the membership values in the condition of the rule. The inference engine utilizes aggregation, activation and accumulation. For the controller used in this paper, the activation operator is based on minimum values, and the accumulation operator is based on maximum values.

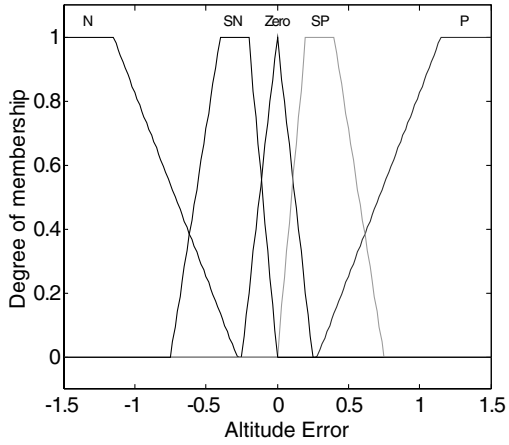

Fig. 6 Membership functions for drogue altitude error.

Defuzzification: In the defuzzification step, the resulting fuzzy set is converted into a numerical value that is used in the control signal. Several defuzzification methods are available, but in this paper, the centroid of area method is employed. The output value is determined by the abscissa of the centroid of the fuzzy set.

Postprocessing: In the postprocessing step, the output value from the fuzzy control algorithm is scaled to appropriate dimensions. In this work, the maximum expected output from the fuzzy controller is scaled to be equal to the maximum permissible control input, in this case the maximum length rate.

IV. Numerical Results

A. Transitional Dynamics

The optimal cable configuration shown in Table 2, taken from [27], is used throughout the following analysis. The parameters were optimized for a light aircraft subject to certain operational constraints so as to minimize the orbit radius of the drogue during circular flight.

The first set of results in this section considers the scenario where the aircraft performs an instantaneous transition from straight flight to circular flight. Two simulations were performed with the damping constant of the cable material set to 500, and one with no cable damping. The aim is to assess whether the damping properties of the material can play a role in the overall dynamics of the maneuver. The aircraft is initially flying straight, and circular flight is initialized after 50 s. Figure 7 shows a close-up of the cable tension variation in the cable segment that becomes slack during the maneuver. It can be seen that damping does not affect the tension significantly, and that both cases predict a slack cable. When the cable becomes taut again, there

Table 1 Rules for cable deployment/retrieval

		Change in altitude error		
		N	Zero	*P*
Altitude error	*N*	*P*	*P*	Zero
	SN	SP	SP	Zero
	Zero	*P*	Zero	*N*
	SP	Zero	SN	SN
	P	Zero	*N*	*N*

Table 2 Optimal system parameters for cable-system

Parameter	Value
Cable length	3000 m
Cable diameter	2.36 mm
Drogue mass	50 kg
Drogue C_DA	2 m^2
Aircraft final orbit radius	221 m
Aircraft velocity	51.5 m/s

are some high frequency oscillations in the tension. With cable damping, these oscillations damp out very quickly. Therefore, inclusion of damping into the simulations does not affect the main dynamical features of the system and is used in the remaining results because of the improved efficiency of the numerical integration.

Figure 8 shows a complete time history of the tension variation during the instantaneous transition. This type of transition is characterized by multiple peaks and troughs in the tension, which eventually damp to a steady-state tension value. Figure 9 shows the cable shape relative to the aircraft after the circle is first initiated. As can be seen, the drogue is initially at a very high altitude (2400 m), being towed some considerable distance behind the aircraft (2991 m). Initiating circular flight with the cable in this configuration (i.e., pulling extremely tight circles) causes significant disruption to the equilibrium configuration. In particular, the relative velocity of the cable closest to the aircraft changes almost immediately, creating a tension wave that travels rapidly down the cable. The immediate loss of tension causes the drogue to lose altitude. However, during the portion of circular flight when the aircraft is flying in its original direction, the tension peaks again causing the drogue altitude to level out somewhat. This process continues as the aircraft circles, and the drogue oscillates as it makes its way to the center of the circle. This is clearly illustrated in Fig. 10. The radius of the drogue's final orbit is on the order of 3.53 m, which agrees excellently with the optimal radius of 3.54 m determined in [27]. It is also apparent that the system is quite stable in a nonlinear sense because the disturbance from the equilibrium condition is significant. However, it takes some time before the drogue oscillations damp out completely (approximately 10 min).

The effect of different transition parameters was examined by comparing the results from several simulations. Note that an exhaustive study was not undertaken. Instead, a qualitative understanding of the general behavior of the system is desired to provide insight into how the tow-in maneuver should be optimized. The different scenarios are listed in Table 3. In each case, the final orbit radius of the aircraft is 221 m. As seen in the preceding results, the variation in the cable tension provides insight into the behavior of the system. In particular, tension values approaching zero with large transient oscillations indicate that the aircraft is transitioning too rapidly to circular flight. Figure 11 shows the time histories of the tension at the drogue end for the different test cases. Cases 2 and 3 are

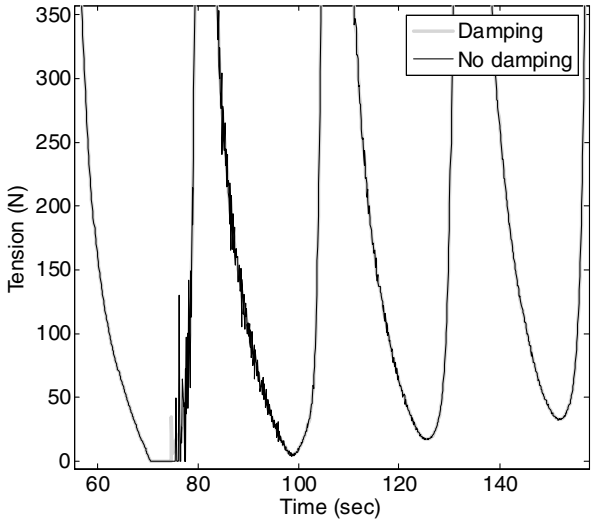

Fig. 7 Tension comparison in element that becomes slack for cable with and without damping.

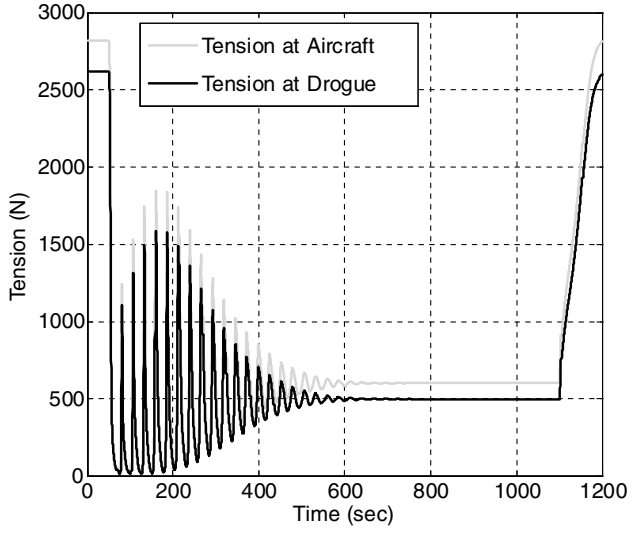

Fig. 8 Cable tension during instantaneous transition to circular flight.

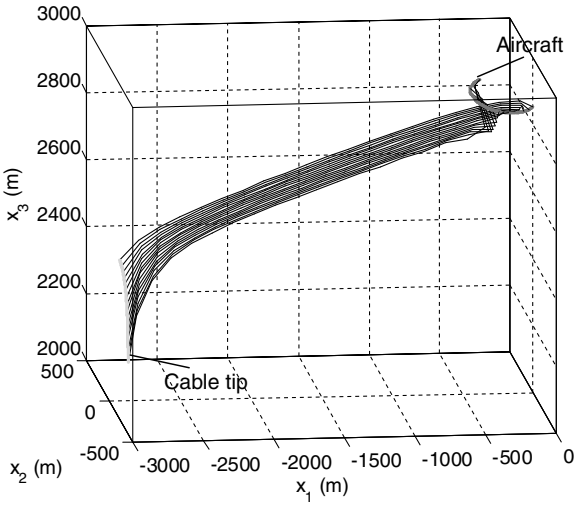

Fig. 9 Cable shape during slack period of instantaneous transition.

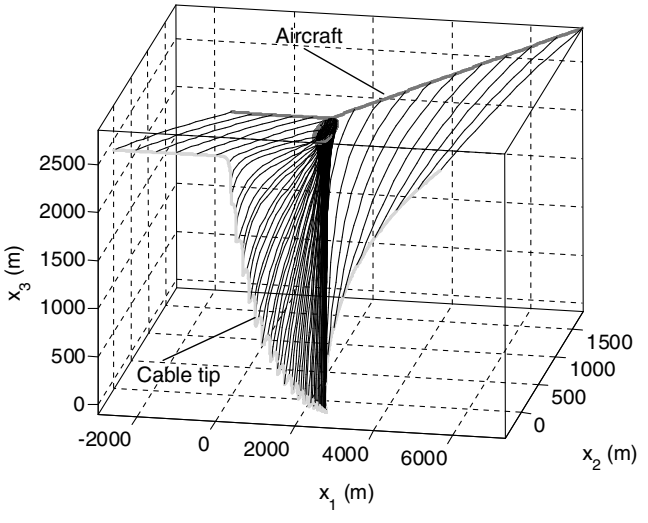

Fig. 10 Cable shape during instantaneous transition to circular flight.

Table 3 Transition parameters for circular flight

Case	Tow-in maneuver begins (initial radius)	Transition ends, circular flight begins	Tow-out maneuver begins	Resume straight flight (final radius)
1	50 s (1500 m)	1050 s	1550 s	1950 s (6000 m)
2	50 s (800 m)	450 s	1050 s	1450 s (6000 m)
3	50 s (800 m)	250 s	750 s	950 s (3000 m)
4	50 s (1200 m)	450 s	1050 s	1450 s (4000 m)
5	50 s (1000 m)	450 s	1050 s	1450 s (5000 m)
6	50 s (1000 m)	350 s	950 s	1350 s (4000 m)
7	50 s (2000 m)	350 s	950 s	1350 s (4000 m)

not particularly good sets of parameters because of the large gradient in tension followed by reasonably large oscillations. In contrast, case 1 appears to have excellent transient dynamics, with minimal tension undershoot and rapid damping of tension oscillations. Case 1 also takes the longest transition time, meaning that the drogue does not reach a steady-state tow radius for several minutes. However, the tip approaches the vicinity of the desired area relatively quickly. Case 5 also appears to have minimal tension fluctuations, but has a much faster convergence to the final tow radius. Figure 11 also shows that the tow-out maneuver is not particularly sensitive to the choice of parameters, and that there is very little danger in terms of transient cable dynamics.

Figures 12 and 13 show the aircraft and drogue trajectories during transition for cases 1 and 5, respectively. A comparison of Fig. 12 with Fig. 10 shows that the drogue spirals downwards towards the target, as opposed to being "pulled" in. The major difference in the dynamics can be traced to the position of the drogue when the aircraft commences turning sharply. In the results shown in Fig. 10, the drogue is directly behind the aircraft at a distance of nearly 3 km when the aircraft commences circling. However, by starting with very large circles, the drogue is gradually pulled into the circle. If the maneuver is timed correctly, the aircraft commences circling at the desired radius when the drogue is nearly at the center of the circle. Hence, this causes the drogue to be towed in progressively smaller radius circles while the drogue descends naturally. Notice the large difference in the altitude of the drogue in straight flight and circular flight. In this particular case, the required aircraft altitude to obtain a ground level position for the drogue was known. Without this knowledge, it is clear that it would be possible for the drogue to impact the ground if the aircraft is flying too low in straight flight. Figure 13 shows the trajectories for case 5, with a significantly faster convergence to the desired altitude and position of the drogue. The drogue converges more quickly to the desired altitude with fewer orbits on its spiral down towards ground level.

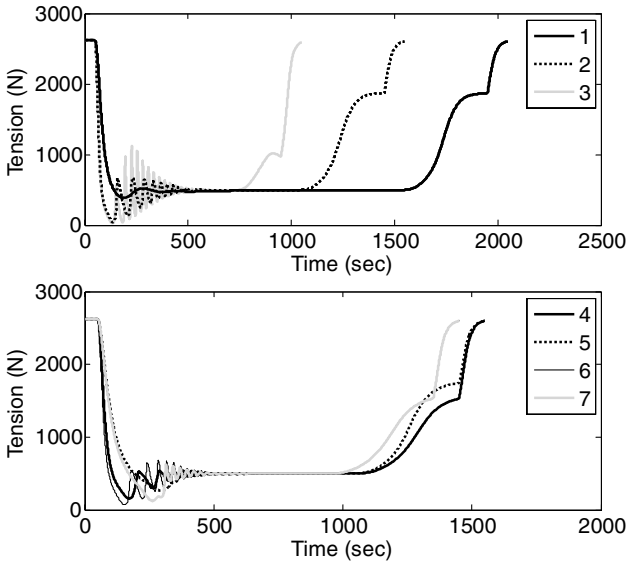

Fig. 11 Effect of transitional parameters on tension variation (drogue end).

These results make it clear that it is important to control the transition of the aircraft from straight flight to circular flight to minimize the possibility of the cable becoming slack and to accelerate the convergence of the drogue towards the center of the circle. The results presented here are probably far from optimal and performing a parameter optimization for the given system is essential to obtain a good combination of fast transition and minimal tension fluctuations. Another possibility would be to have the aircraft climb into a circle from a lower altitude, but this is not considered here.

B. Transition Maneuver Optimized via Simulated Annealing

An optimal tow-in maneuver was determined using the strategy discussed in Section III.B. The aircraft controls (power, lift coefficient, and bank angle) are computed via a root-finding technique using the aircraft accelerations, tension components, and aircraft aerodynamics expressed in cylindrical coordinates [27]. Figure 14 shows projections of the cable shape, together with the aircraft and cable tip paths. Figure 15 shows the variation in orbit radius for the optimal transition. The initial orbit radius is 1510 m and the transition time is 389.1 s. The orbit radius varies very smoothly during the optimized transition and is similar in many respects to a cosine-variation. Figure 15 also shows the minimum tension in the cable for the optimized tow-in maneuver, demonstrating a smooth transition with fast convergence of the cable tip to the desired altitude.

Figure 16 shows the computed aircraft controls necessary to fly the optimal transition maneuver. The power required is a maximum at the initial time, which is due largely to the high tension applied at the aircraft. In other words, the power required is dictated by the requirements for straight flight. This is in excess of that used to optimize the circular-flight trajectory, and hence, it would be necessary to fly the aircraft with the cable only partially deployed. The required power decreases during the transition because of the significant drop in tension, and increases as the final orbit radius is approached. The required lift coefficient begins at approximately 0.719 and increases relatively smoothly to the final value of 1.1. The

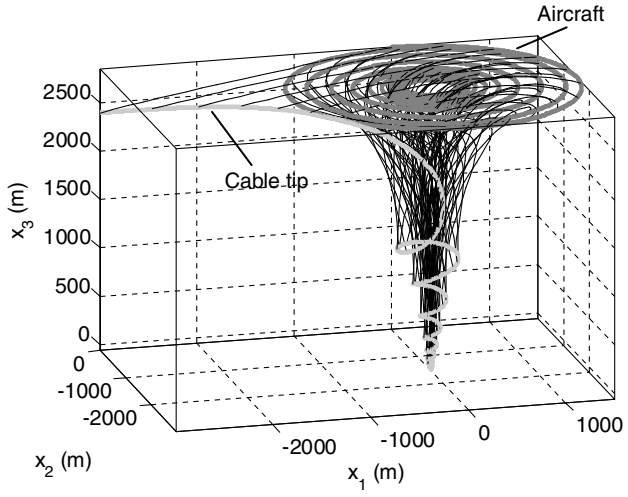

Fig. 12 Cable shape, aircraft and drogue trajectories for case 1.

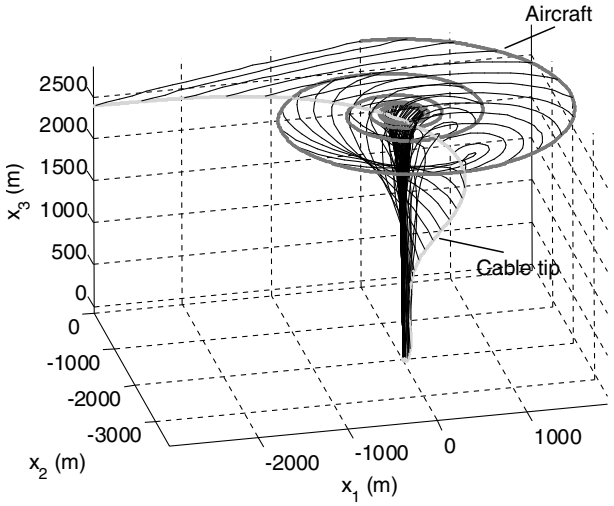

Fig. 13 Cable shape, aircraft and drogue trajectories for case 5.

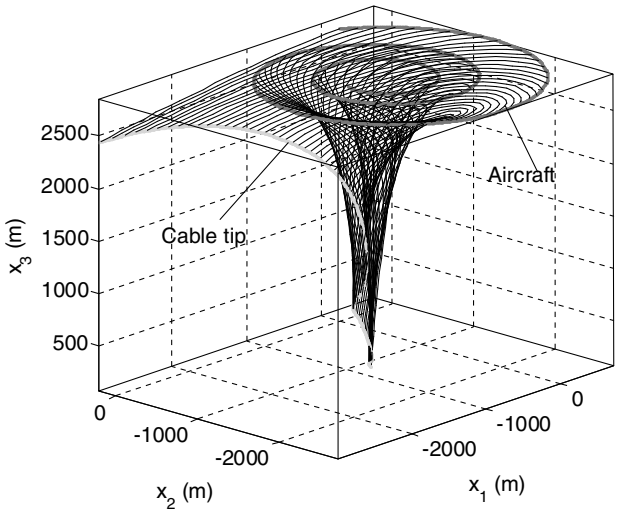

Fig. 14 Cable shape, aircraft and drogue trajectories for optimized tow-in maneuver.

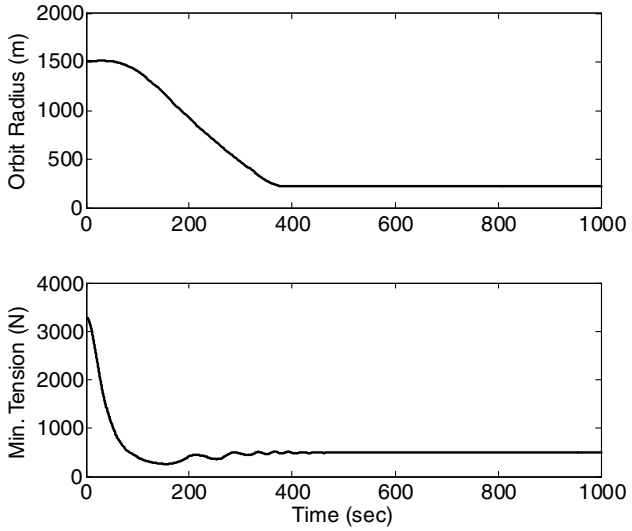

Fig. 15 Variation in orbit radius and minimum cable tension during optimal transition.

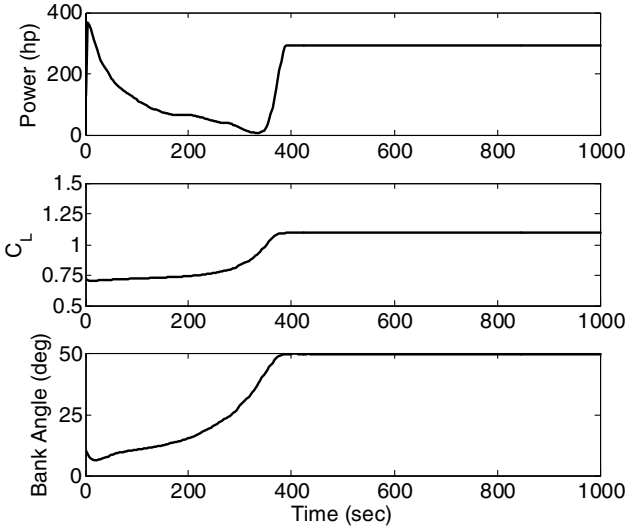

Fig. 16 Aircraft controls required for optimal transition maneuver.

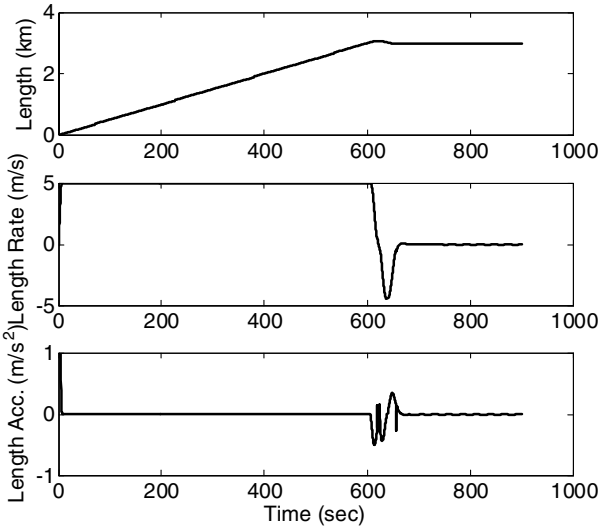

Fig. 17 Deployment dynamics of cable during circular flight.

bank angle for the initial orbit radius of 1510 m is approximately 10.1 deg, which increases smoothly to the bank angle required for the pure circular flight (50 deg).

C. Deployment Dynamics

In this section, we focus our attention on the cable deployment dynamics during circular flight. In all of the following results, the cable is initially at a length of 0.5 m and the aircraft is at an altitude of 2950 m. The cable length rate is initially zero and the drogue is in equilibrium. The final desired altitude of the drogue is 1.5 m above the ground. The maximum permissible length rate is set to 5 m/s and the maximum reel acceleration is set to 1 m/s^2. The control gains are kept constant at $k_1 = 1.5$ and $k_2 = 0.05$. The cable configuration is the same as that given in Table 2, and the discretization of the cable is 40 segments when fully deployed.

1. Heuristic Deployment Control

In this study, some of the key parameters in the heuristic deployment controller are held fixed. The transition altitude is set as $\Delta h_t = 60$ m, and the critical altitude is set as $\Delta h_c = 10$ m. The influence of the deployment rate was studied by simply commanding the drogue to an altitude of 40 m. The length variation, length rate, and control input are shown in Fig. 17. The first thing to note is that

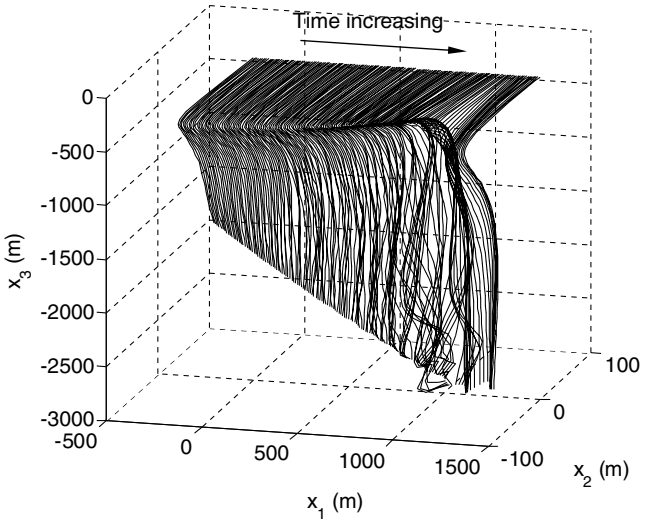

Fig. 18 Cable shape viewed from rotating frame during deployment showing lateral instability.

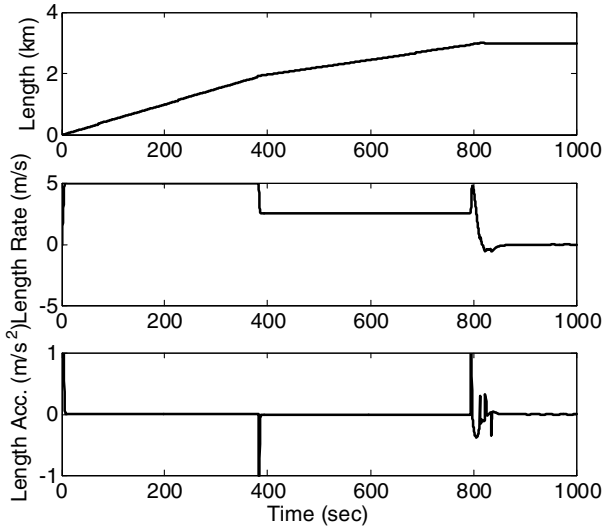

Fig. 19 Deployment dynamics of cable during circular flight with modified deployment scheme.

the deployment takes place at the maximum rate for the majority of the deployment. It can also be seen that there is an overshoot in cable length at the end of deployment. The instability caused by deploying the cable too quickly at long lengths is illustrated in Fig. 18. In this particular case the lateral excitation is quite severe. The amplitude of the oscillations from the cable equilibrium position are on the order of 60 m. The instability decreases and eventually disappears when the deployment ceases. The instability is a physical effect and occurs predominantly in the radial direction of the circle. Although the exact cause is not known, it is likely to be due to the large gradient in forces on the cable when the cable length exceeds a given threshold. For example, when the cable length is short, the cable is largely straight and subjected to large drag forces. As the length increases, the drogue approaches the center of the circle and the lower part of the cable becomes vertical, whereas the upper portion of the cable remains at a significant angle to the vertical. In other words, the cable takes on a significant curvature. As the cable is deployed, the upper portion is subjected to large drag and large centripetal forces because of its distance from the center of rotation. However, the lower portion of the cable is closer to the center of the circle and is subjected to less drag and lower centripetal forces. When the cable is deployed quickly, the portions subjected to large forces move towards regions with lower forces. The sudden change in force due to cable curvature is the likely cause of the excitation of the lateral modes. However, more detailed study is required to verify this conjecture.

To illustrate that the lateral instability is due to too high deployment velocities at long lengths, a second scenario with the critical length set to $L_{\text{crit}} = 1900$ m and the maximum deployment rate in the second phase set to 2.5 m/s was performed. The length dynamics are shown in Fig. 19, and the resulting cable shape at the end of deployment is shown in Fig. 20. Comparing Fig. 20 with Fig. 18 shows that slowing the deployment causes a significant reduction in the amplitude of the lateral vibration modes. Although the vibrations are not completely eliminated, the instability is less likely to be a hazard to the system.

A complete deployment simulation is shown in Figs. 21–23 (i.e, deployment to 1.5 m altitude). In this scenario, the critical length is set to $L_{\text{crit}} = 1500$ m, and the new maximum deployment rate is 2.5 m/s. Figure 21 shows the variation in length, length rate, and length acceleration. Note that there is an intentional increase in the length rate from the maximum of 2.5 m/s at the end of the first deployment phase. Figure 22 shows the cable shape during the final stages of deployment, clearly showing the significant reductions in lateral cable modes. For further validation of the theory that large deployment rates cause the excitation of lateral modes, the peak in the length rate at the end of the deployment is labeled in Fig. 22. The cable shape in this region shows signs of a lateral wave being created. However, because the length rate is large for only a short time, the

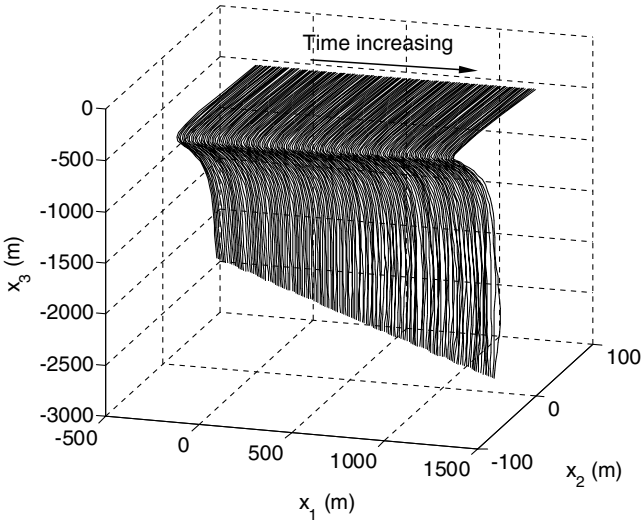

Fig. 20 Cable shape viewed from rotating frame during deployment showing reduction in lateral instability.

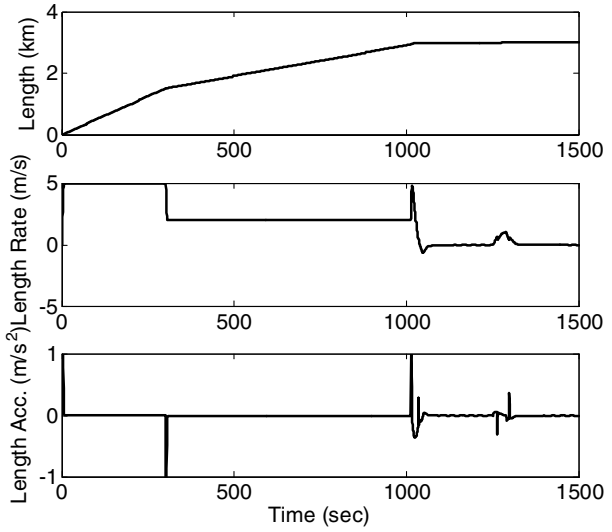

Fig. 21 Deployment dynamics of cable during circular flight with complete deployment scheme.

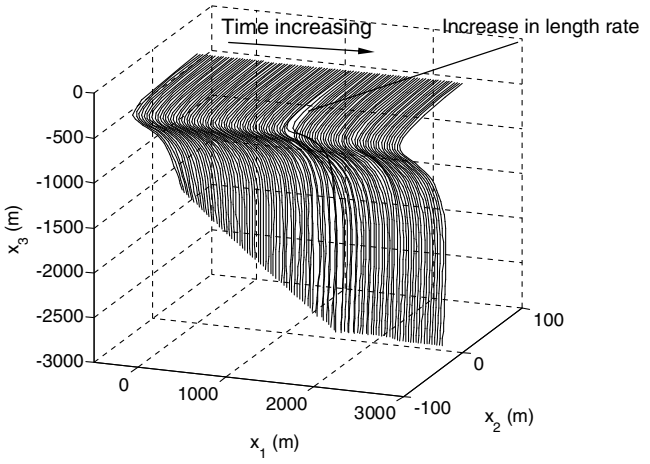

Fig. 22 Cable shape viewed from rotating frame during deployment for complete deployment.

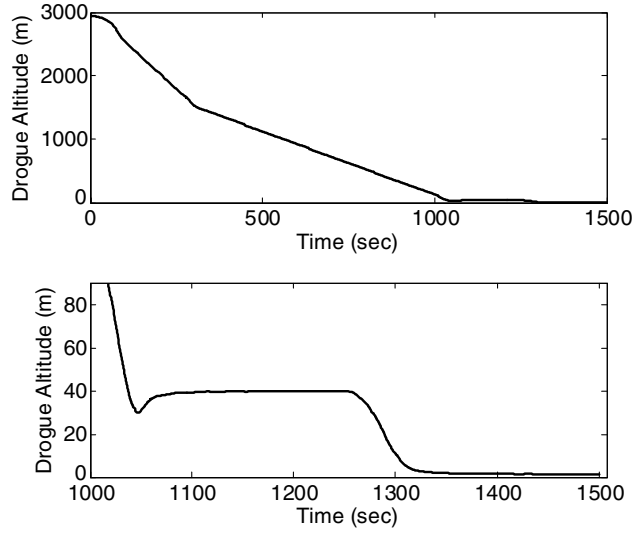

Fig. 23 Drogue altitude during deployment: overall (top) and close-up of final variation (bottom).

lateral wave does not grow. Figure 23 shows the time variation of the drogue altitude during the deployment. The most important aspect of Fig. 23 is the final convergence of the drogue altitude. The drogue stabilizes to $h_0 = 40$ m at approximately 1100 s, and the final altitude of 1.5 m is commanded with a linear variation beginning at 1250 s and terminating at 1290 s. Figure 23 illustrates that the convergence to the desired altitude is very good, and the drogue does not impact the ground.

2. Fuzzy Logic Deployment Control

Deployment simulations using the fuzzy logic controller were conducted for various situations. However, the deployment results presented here are for a specific case where the commanded drogue altitude is initially 40 m. At 850 s, a linear variation in the commanded altitude to the final altitude of 1.5 m is used over a time interval of 90 s. The results from this simulation are shown in Figs. 24–26. Figure 24 shows the variation in length, length rate, and length acceleration. Several points are evident upon comparing Fig. 24 with Fig. 19 or 21. First, the initial control input and reel rate are very similar for both cases, showing that a good proportion of the deployment is completed at the maximum rate. After approximately 300 s (cable length 1500 m), the deployment rate begins to decrease to a rate of about 3.44 m/s. The length rate then decreases almost logarithmically until the initial desired altitude of 40 m is achieved. The length rate then peaks again at about 0.43 m/s during the final

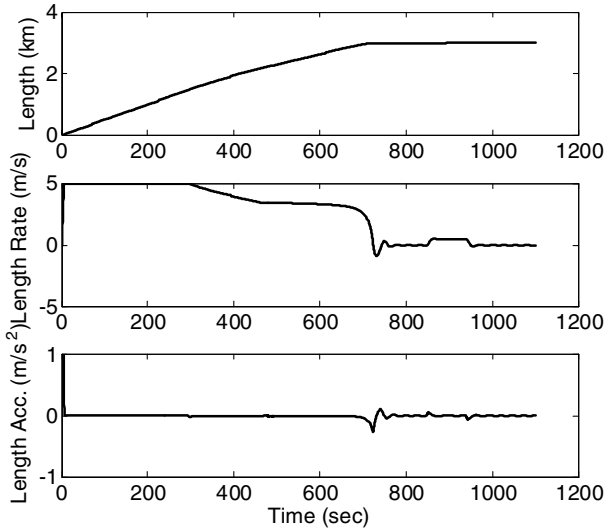

Fig. 24 Length dynamics using fuzzy logic deployment controller.

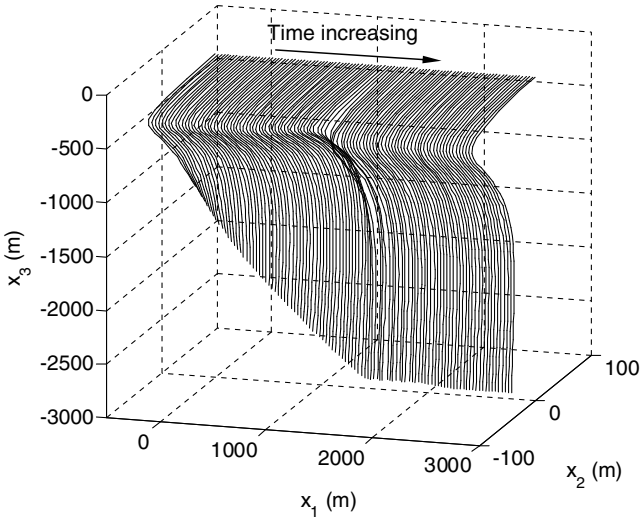

Fig. 25 Cable shape during final stages of deployment with fuzzy logic deployer.

deployment stage until the drogue reaches 1.5 m altitude. The required length acceleration is considerably less than the heuristic controller, with saturation only at the initial time. Hence, deployment with this controller is generally smoother.

The cable shape during deployment with the fuzzy logic controller is shown in Fig. 25. It is apparent that the cable shape is maintained very well compared with the heuristic deployment scheme. There are no lateral oscillations present in the cable during this deployment. Thus, this particular deployment scheme may be the best choice for such a system because it seems to naturally attend to the lateral cable dynamics due to a reduction in the length rate as the final altitude is approached. Figure 26 shows the variation in the drogue altitude during the deployment, with a close-up of the final stages. It can be seen that the deployer tends to overdeploy the cable slightly, causing an undershoot in drogue altitude. However, the controller is adequately able to remove any steady-state errors in altitude and demonstrates good closed-loop stability. The drogue does not impact the ground using the two-stage deployment scheme proposed here.

V. Conclusions

Circularly towed cable systems have potential applications for remote payload pickup and delivery. Two important aspects of the

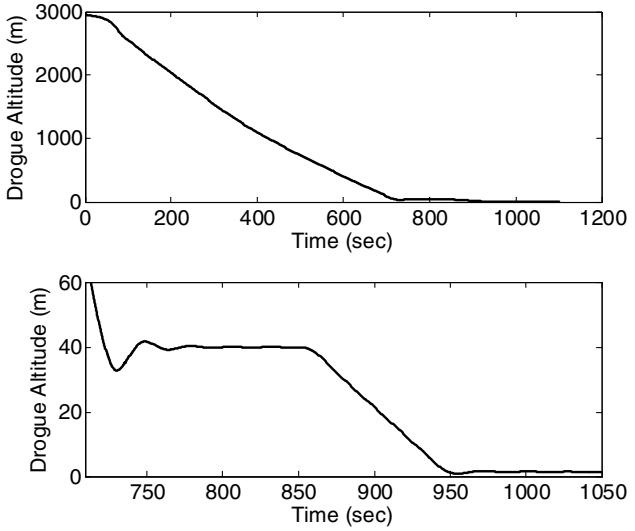

Fig. 26 Deployment with fuzzy logic: overall (top) and close-up of final variation (bottom).

dynamics of such a system were examined. First, because it may be preferable to get into and out of a remote region quickly, flying an aircraft with the cable already deployed before entering into circular flight may be desirable. However, special attention must be given to the transitional flight regime to prevent the cable from becoming slack and to make the drogue approach the desired state quickly. It was demonstrated through numerical simulations that the transitional phase can be adjusted to satisfy these objectives. The transitional phase was optimized to ensure fast convergence of the cable tip to the desired location using simulated annealing. Another alternative is to simply deploy the cable from a circling aircraft. Two deployment schemes were used, implemented via control of the winch acceleration. A new instability of the cable lateral modes has been identified due to large cable deployment rates when the cable is beyond a critical length. The instability can be significantly reduced by adjusting the deployment rate as a function of the deployed length. A fuzzy logic deployment scheme, which naturally reduces the deployment rate as the drogue approaches the target, provides good closed-loop performance while suppressing the lateral cable vibrations.

References

[1] Trivailo, P., Blanksby, C., Sgarioto, D., Williams, P., and Smart, R., "Defence Applications for Cable Systems Deployed from Aerial and Naval Platforms," *Proceedings of the Land Warfare Conference*, edited by V. Puri, D. Filippidis, S. Quinn, and J. Kelly, Defense Science and Technology Office, Edinburgh, South Australia, 2003, pp. 285–294.

[2] Hambling, D., "Throw Me a Rope," *New Scientist*, Vol. 2497, April 2005, pp. 35–37.

[3] Huffman, R. R., and Genin, J., "The Dynamical Behaviour of a Flexible Cable in a Uniform Flow Field," *The Aeronautical Quarterly*, Vol. 23, May 1971, pp. 183–195.

[4] Phillips, W. H., "Theoretical Analysis of Oscillations of a Towed Cable," NACA TN-1796, Jan. 1949.

[5] Genin, J., Citron, S. J., and Huffman, R. R., "Coupling of Longitudinal and Transverse Motions of a Flexible Cable in a Uniform Flow Field," *The Journal of the Acoustical Society of America*, Vol. 52, No. 1, 1972, pp. 438–440.

[6] Norris, S. R., and Andrisani, D., "Longitudinal Equilibrium Solutions for a Towed Aircraft and Tow Cable," AIAA Paper 2001-4254, Aug. 2001.

[7] Nakagawa, N., and Obata, A., "Longitudinal Stability Analysis of Aerial-Towed Systems," *Journal of Aircraft*, Vol. 29, No. 6, 1992, pp. 978–985.

[8] Etkin, B., "Stability of a Towed Body," *Journal of Aircraft*, Vol. 35, No. 2, 1998, pp. 197–205.

[9] Jones, S. P., and Krausman, J. A., "Nonlinear Dynamic Simulation of a Tethered Aerostat," *Journal of Aircraft*, Vol. 19, No. 8, 1982, pp. 679–686.

[10] Lambert, C., and Nahon, M., "Stability Analysis of a Tethered Aerostat," *Journal of Aircraft*, Vol. 40, No. 4, 2003, pp. 705–715.

[11] Cochran, J. E., Innocenti, M., No, T. S., and Thukral, A., "Dynamics and Control of Maneuverable Towed Flight Vehicles," *Journal of Guidance, Control, and Dynamics*, Vol. 15, No. 5, 1992, pp. 1245–1252.

[12] Henderson, J. F., Potjewyd, J., and Ireland, B., "The Dynamics of an Airborne Towed Target System with Active Control," *Proceedings of the Institution of Mechanical Engineers, Part G: Journal of Aerospace Engineering*, Vol. 213, No. 5, 1999, pp. 305–319.

[13] Bourmistrov, A. S., Hill, R. D., and Riseborough, P., "Nonlinear Control Law for Aerial Towed Target," *Journal of Guidance, Control, and Dynamics*, Vol. 18, No. 6, 1995, pp. 1232–1238.

[14] Quisenberry, J. E., and Arena, A. S., "Dynamic Simulation of Low Altitude Aerial Tow Systems," AIAA Paper 2004-4813, Aug. 2004.

[15] Lawhon, R. D., and Arena, A. S., "Design Considerations for an Aerially Towed Vehicle with Altitude Holding Capability," AIAA Paper 2004-4812, Aug. 2004.

[16] Jun, Y.-W., Hall, K. R., Bennett, A. G., and Bridges, P. D., "Optimal Guidance for Airborne Cable Pickup System," AIAA Paper 84-1893, Aug. 1984.

[17] Trivailo, P., Sgarioto, D., and Blanksby, C., "Optimal Control of Aerial Tethers for Payload Rendezvous," *The 5th Asian Control Conference*, Vol. 1, IEEE Publications, Piscataway, NJ, 2004, pp. 396–404.

[18] Williams, P., Sgarioto, D., and Trivailo, P., "Optimal Control of an Aircraft-Towed Flexible Cable System," *Journal of Guidance, Control, and Dynamics* (to be published).

[19] Murray, R. M., "Trajectory Generation for a Towed Cable System using Differential Flatness," *IFAC World Congress*, Pergamon, New York, 1996, pp. 395–400.

[20] Hover, F. S., "Inversion of a Distributed System for Open-Loop Trajectory Following," *International Journal of Control*, Vol. 60, No. 5, pp. 671–686.

[21] Borst, R. G., Greisz, G. F., and Quynn, A. G., "Fuzzy Logic Control Algorithm for Suppressing E-6A Long Trailing Wire Antenna Wind Shear Induced Oscillations," AIAA Paper 93-3868, Aug. 1993.

[22] Brushwood, D. L. J., Olson, A. P., and Smyth, J. M., "The E-6A Orbit Improvement System and its Effect Upon LTWA Verticality," AIAA Paper 98-4426, Aug. 1998.

[23] Frost, G., and Costello, M., "Improved Deployment Characteristics of a Tether-Connected Munition System," *Journal of Guidance, Control, and Dynamics*, Vol. 24, No. 3, 2001, pp. 547–554.

[24] O'Donnell, J., "Air Pick-Up," *EnRoute*, Vol. 9, No. 1, 2000, available on-line at http://www.postalmuseum.si.edu/resources/6a2w_airpick-up.html [cited 20 July 2006].

[25] Purvis, P., "Fulton's Skyhook: An Early Method of Crew Extraction," *Flight Journal*, Sept.–Oct. 2004, available on-line at http://www.flightjournal.com/fj/articles/skyhook/skyhook.asp [cited 20 July 2006].

[26] Boyne, W. J., "The Awesome Power of Air Force Gunships," *Air Force Surveys in Geophysics*, Vol. 82, No. 4, 1999, pp. 78–84.

[27] Williams, P., and Trivailo, P., "Dynamics of Circularly Towed Aerial Cable Systems, Part 1: Optimal Equilibrium Configurations and Their Stability," *Journal of Guidance, Control, and Dynamics* (to be published); also AIAA Paper 2005-6124, Aug. 2005.

[28] Schram, J. W., and Reyle, S. P., "A Three-Dimensional Dynamic Analysis of a Towed System," *Journal of Hydronautics*, Vol. 2, No. 4, 1968, pp. 213–220.

[29] Ablow, C. M., and Schechter, S., "Numerical Simulation of Undersea Cable Dynamics," *Ocean Engineering*, Vol. 10, No. 6, 1983, pp. 443–457.

[30] Roberts, G. M., Connell, H. J., and May, R. L., "A Three Dimensional Model of a Towed Cable-Body System," RMIT Dept. of Mathematics Research Rept. 14, Aug. 1994.

[31] Chin, C. K. H., May, R. L., and Connell, H. J., "A Numerical Model of a Towed Cable-Body System," *ANZIAM Journal*, Vol. 42, Pt. E, 2000, pp. C362–C384.

[32] Pai, P. F., and Nayfeh, A. H., "Fully Nonlinear Model of Cables," *AIAA Journal*, Vol. 30, No. 12, 1992, pp. 2993–2996.

[33] Leonard, J. W., and Nath, J. H., "Comparison of Finite Element and Lumped Parameter Methods for Oceanic Cables," *Engineering Structures*, Vol. 3, No. 3, 1981, pp. 153–167.

[34] Driscoll, R., and Nahon, M., "Mathematical Modeling and Simulation of a Moored Buoy System," *Proceedings of IEEE Oceans*, Vol. 1, Sept. 1996, pp. 517–523.

[35] Buckham, B., Nahon, M., and Seto, M., "Three-Dimensional Dynamics Simulation of a Towed Underwater Vehicle," American Society of Mechanical Engineers Paper 99-3068, 1999.

[36] Winget, J. M., and Huston, R. L., "Cable Dynamics—A Finite Segment Approach," *Computers and Structures*, Vol. 6, No. 6, 1976, pp. 475–480.

[37] Kamman, J. W., and Huston, R. L., "Modeling of Variable Length Towed and Tethered Cable Systems," *Journal of Guidance, Control, and Dynamics*, Vol. 22, No. 4, 1999, pp. 602–608.

[38] Banerjee, A. K., and Do, V. N., "Deployment Control of a Cable Connecting a Ship to an Underwater Vehicle," *Applied Mathematics and Computation*, Vol. 70, Nos. 2–3, 1995, pp. 97–116.

[39] Dreyer, T., and Murray, D. M., "On the Modeling of Two-Dimensional Segmented Representations of Cable Shape," *Ocean Engineering*, Vol. 11, No. 6, 1984, pp. 609–625.

[40] Choo, Y.-I., and Casarella, M. J., "A Survey of Analytical Methods for Dynamic Simulation of Cable-Body Systems," *Journal of Hydronautics*, Vol. 7, No. 4, 1973, pp. 137–144.

[41] Williams, P., and Trivailo, P., "Cable Deployment Control for Towed Aerial-Cable Payload Pick-Up and Delivery System," *Proceedings of the Land Warfare Conference*, edited by V. Puri, D. Filippidis, P. Retter, and J. Kelly, Defense Science and Technology Office, Edinburgh, South Australia, 2004, pp. 313–329.

[42] King, R. E., *Computational Intelligence in Control Engineering*, Marcel Dekker, New York, 1999.

[43] Zadeh, L. A., "Fuzzy Sets," *Information and Control*, Vol. 8, No. 3, 1965, pp. 338–353.